Effects of Oxygen Plasma on the Chemical, Light-emitting, and Electrical Transport Properties of Inorganic and Hybrid Lead Bromide Perovskite Nanocrystal Films

Francisco Palazon,[†§*] Fang Chen,[†] Quinten A. Akkerman,[†] Muhammad Imran,[†] Roman Krahne,[†] and Liberato Manna[†*]

[†] Nanochemistry Department, Istituto Italiano di Tecnologia, Via Morego 30, 16163 Genova, Italy

[§] Instituto de Ciencia Molecular, ICMol, Universidad de Valencia, C/ Catedrático J. Beltrán 2, 46980 Paterna, Spain

Keywords: Perovskite, nanocrystals, plasma, optoelectronics, photoluminescence, conductivity

ABSTRACT

We show that oxygen plasma affects in different ways the structural, chemical, optical and electrical properties of methylammonium and cesium lead bromide nanocrystals. Hybrid organic-inorganic nanocrystals were severely and quickly degraded by oxygen plasma at 50 W. Their photoluminescence was quenched with almost 100% loss of initial quantum yield. This is linked to the decomposition of the nanocrystals. Inorganic nanocrystals were more resistant to oxygen plasma in the same conditions. Despite a moderate loss of photoluminescence and electrical conductivity, oxygen plasma had a positive impact, removing unbound ligands resulting in a more ohmic behavior of the film. This paves the way to the application of oxygen plasma in the development of perovskite-based optoelectronic devices.

Lead halide perovskite nanocrystals (LHP NCs) are being increasingly used as active materials in different optoelectronic devices such as light-emitting diodes (LEDs)[1–9] and solar cells.[10–14] Although it is possible to fabricate these devices fully by solution processes,[15] it is also common to employ plasma-assisted processes such as plasma-enhanced chemical vapor deposition (PECVD) or plasma-enhanced atomic layer deposition (PEALD) for the formation of various layers acting as charge extraction materials or antireflective coatings.[16–18] For perovskite devices, plasma-assisted processes have been used for the deposition of bottom layers of TiO_2[19–21] and SnO_2.[22] Xiao *et al.* have also demonstrated the beneficial use of argon plasma directly on perovskite films[23] while others have grown protective alumina layers on perovskites by ALD.[24] However, to the best of our knowledge no report on the use of oxygen plasma on perovskites has been published so far. This is likely linked to the high sensitivity of perovskites towards multiple external agents. Numerous works have detailed the evolution (in many cases degradation) of LHP NCs exposed to water, air, thermal annealing, and several chemicals such as amines, thiols, and different halide anion sources.[25–31] Hereafter we detail the structural, chemical, optical and electrical properties of hybrid methylammonium lead tribromide ($MAPbBr_3$) and fully-inorganic cesium lead tribromide ($CsPbBr_3$) colloidal NCs deposited as thin films, exposed to oxygen plasma for varying amounts of time, and used in simple planar devices with top-contacted electrodes (see Scheme 1).

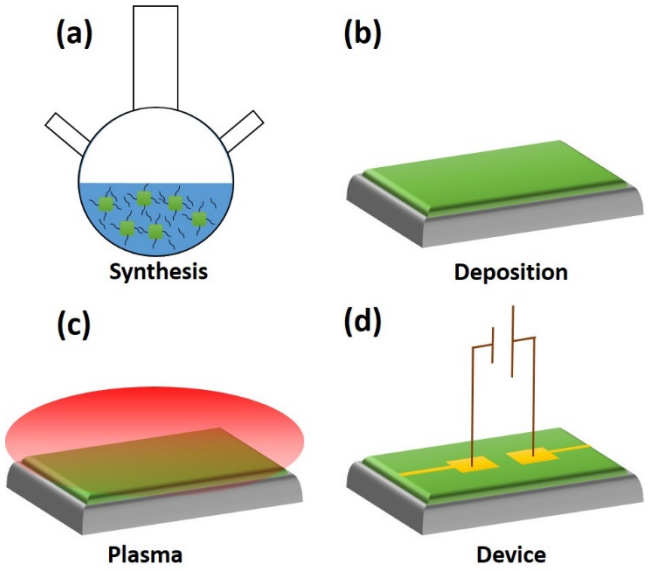

Scheme 1. Schematic representation of the process studied here involving (a) colloidal synthesis of lead bromide NCs passivated with surfactants bearing long aliphatic chains; (b) deposition of these NCs on a substrate by drop-casting or spin-coating; (c) exposure of the film to oxygen plasma for different times and (d) evaluation of the photoluminescence (not shown in the scheme) and electrical conductivity on a simple device with top-contacted electrodes.

Colloidal $CsPbBr_3$ and $MAPbBr_3$ NCs where synthesized by a previously reported hot-injection method with benzoyl bromide precursor.[32] The optical characterization of both NCs in solution and TEM images of drop-casted NCs are presented in Figure S1, showing good size and shape monodispersity as well as strong absorption onsets around 510 nm - 525 nm and corresponding Stokes-shifted photoluminescence (PL). In order to investigate the chemical and structural stability upon exposure to oxygen plasma of these NCs, both solutions were drop-cast on zero-diffraction silicon wafers. After drying in vacuum, the samples were exposed to oxygen plasma for different amounts of time at the same operation conditions (see Experimental Section for more details) and were analyzed by X-ray diffraction (XRD) and X-ray photoelectron spectroscopy (XPS), as reported in Figure 1.

XRD analyses (Figure 1a,b) show that in both cases the NCs retain their crystalline structure, corresponding to orthorhombic $CsPbBr_3$ (ICSD 97851) and cubic $MAPbBr_3$ (ICSD 252415), upon exposure to oxygen plasma. Hence it could be thought that O_2 plasma in these conditions is chemically innocuous to the NC films. Furthermore, the XRD peaks remain broad, as expected from these NCs.[32] Therefore, oxygen plasma does not lead to NC sintering, as is the case of post-deposition thermal annealing processes.[30,31] Despite this apparent insensibility of the NC films towards O_2 plasma, XPS analyses (Figure 1c-e) show significant differences. It must be noted that while XRD probes the whole film (*ca.* 1 micron thick) and is hence less sensitive to changes occurring at the surface, XPS probes only the surface (*ca.* 10 nm). Hence, it appears that O_2 plasma affects mainly the top few nanometers to few tens of nanometers of the film. In the case of $CsPbBr_3$ NCs (Figure 1c,e), the changes at the film surface are minimal. Figure 1c shows that the initial amount of organics in the film, as evaluated by XPS is high (*ca.* 90%). This value is in line with previous reports.[33] It is likely that the surface of the film is especially rich in organics, especially since the film is prepared by drop-casting. This is because as the solvent evaporates, the NCs (which are heavier than single ligand molecules) sediment first, and excess organics (unbound long-chain molecules) remain dissolved in the residual solvent. Once the solvent evaporates entirely, most excess organics are left on top of the NC film. This organic-rich (insulating) film on top of the NCs can be very detrimental for optoelectronic applications, preventing the charge injection/extraction to/from the NC film. These residual organics on $CsPbBr_3$ NC films can be partly removed by oxygen plasma, although the relative percentage of carbon remains rather high (*ca.* 83 %). The Cs:Pb:Br stoichiometry as evaluated by XPS (Figure 1e) appears to show a loss of bromine. Nonetheless, given that the initial composition is Br-rich, we can infer that what is removed is mostly unbound $OlAm^+$-Br^- complexes (in agreement with the depletion of nitrogen seen in Figure 1c). Hence, we can conclude that oxygen plasma is beneficial in this case to clean the film surface without altering the NCs, either at the surface (Figure 1c,e) or in the bulk (Figure 1a).

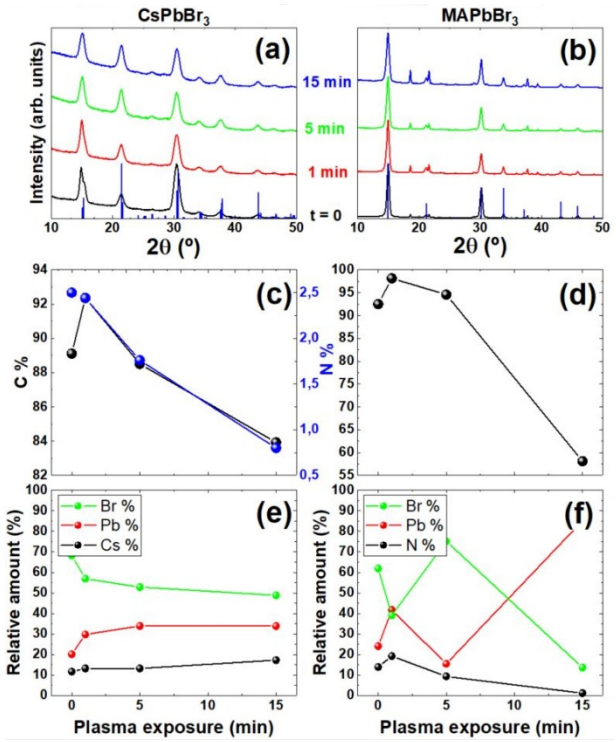

Figure 1. XRD and XPS analyses of drop-cast films exposed to oxygen plasma for different time periods. The left column (a, c, e) presents the evolution of $CsPbBr_3$ NC films while the right column (b, d, f) corresponds to $MAPbBr_3$. XRD diffractograms of both films upon different times of plasma exposure is presented in panels (a) and (b) along with reference patterns for bulk orthorhombic $CsPbBr_3$ (ICSD 97851) and cubic $MAPbBr_3$ (ICSD 252415) represented as blue columns. Panels (c) and (d) present the carbon (black) and nitrogen (blue) atomic percentage of the films versus plasma exposure time. Panels (e) and (f) present the Cs:Pb:Br (e) and N:Pb:Br (f) relative amounts. The data for panels (c-f) is computed from XPS spectra (see Figure S2).

In the case of $MAPbBr_3$ NCs (Figure 1d,f), the changes are more significant, pointing to the higher lability of hybrid NCs. The initial organic content in the film (Figure 1d) is comparable to the one for $CsPbBr_3$ NCs. In the first 5 minutes of oxygen plasma, this amount remains high. During this time, the N:Pb:Br ratio (Figure 1f) is difficult to determine given the low signal of the corresponding peaks (see Figure S2). Nonetheless, the stoichiometry remains reasonably close to the expected 20:20:60 ratios. A large difference is seen at longer times, where the carbon percentage drops significantly to *ca.* 60%. Although it is tempting to attribute this to the removal of unbound ligands, it must be noted that contrary to $CsPbBr_3$, the $MAPbBr_3$ NCs themselves have an organic component. Therefore, an additional reason for such decrease in carbon content can be the degradation of NCs, and more specifically the loss of MA and Br, either in the form of MABr or under other forms, like CH_3NH_2 and HBr, in accordance to previous studies on possible degradation pathways for such LHPs.[34] This degradation is confirmed by looking at the N:Pb:Br ratios (Figure 1f). Indeed, after the first 5 minutes, nitrogen is barely detectable and the bromine content is greatly reduced. Furthermore, the XPS signal for bromine reveals a progressive oxidation from bromide to bromine oxides (see Figure S3). Hence, we can conclude that a prolonged exposure to oxygen plasma at 50 W leads

to loss of MABr and formation of lead and bromine oxides at the surface of the NC film. This higher lability of hybrid LHP NCs can also be seen by XRD on thin films (Figure S4).

In order to evaluate how the chemical evolutions described so far affect the physical properties of these NC films, we prepared spin-coated thin films on glass substrates to perform optical characterizations as well as electrical transport measurements, with gold electrodes deposited on top of the NC films (see the Experimental Section for more details on sample preparation).

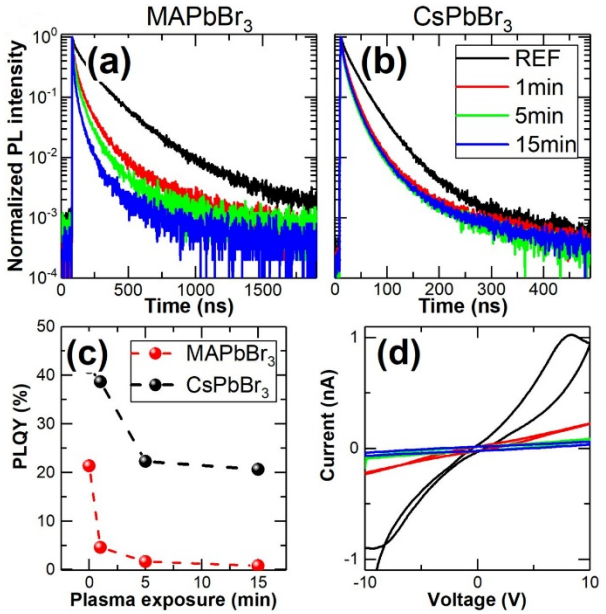

Figure 2. Time traces of the PL intensity decay recorded at the wavelength of maximum PL from $MAPbBr_3$ NC films (a) and $CsPbBr_3$ NC films (b) (note that the time scales span over a different range). Evolution of absolute PLQY values for films of both compositions as a function of plasma exposure time (c), and I-V curves of $CsPbBr_3$ NC films exposed for different times to oxygen plasma (d) (the legend on panel (b) applies for panels a, b, and d).

Figure 2 shows the PL quantum yield (PLQY) and PL decay traces of both films of LHP NCs after exposure to oxygen plasma for different times (see Figure S5 for PL spectra) as well as current-voltage curves for $CsPbBr_3$ NC films. In accordance with the general conclusion from chemical characterization, $MAPbBr_3$ NC films show a much faster and drastic degradation of their PL properties than films of $CsPbBr_3$ NCs. Indeed, the hybrid NC films lose over 75% of their PLQY in the first minute of exposure to oxygen plasma and show barely any PL at all at longer times (PLQY < 1% after 15 minutes; Figure 2c). This is accompanied by a gradual drop in PL lifetime (Figure 2a) pointing to the degradation of the NCs. In contrast, the films of $CsPbBr_3$ NCs retain about 50% of their initial PLQY even after 15 minutes, evidencing their higher stability. Concerning $CsPbBr_3$ PL decay lifetimes, we observe a clear decrease after the first minute of plasma which may be attributed to the formation of non-radiative trap states linked to the removal of surface ligands. However, upon further exposure, PL decay traces remain very similar (as does the PLQY value from 5 min to 15 min) which points to the high stability of fully-inorganic NCs towards oxygen plasma. Figure 2d presents current-voltage curves of $CsPbBr_3$ NC films after different times of plasma exposure (hybrid organic-inorganic NCs were too severely degraded to record reliable electrical transport measurements). The oxygen plasma has an important effect on the electrical transport properties of these NC films. On the reference film before plasma exposure (Figure 2d, black curve) the I-V curve manifests strong hysteretic behavior, and repeated recording of the I-V curves evidences irreproducibility of the traces. Exposing the film to oxygen plasma for 1 minute at 50 W (red curve) leads to much lower currents, but to reproducible and stable I-V curves with only minor hysteresis, and almost ohmic (linear) behavior. A longer exposure (green and blue curves) reduces the conductivity of the NC film further, which indicates that high doses of plasma may eventually degrade the electrical properties of the NC film.

In summary, we have shown that oxygen plasma, as commonly used in different processes involved in device nanofabrication has important effects on LHP NC films. When hybrid organic-inorganic NCs are used, the film undergoes rapid degradation on its top few tens of nanometers under the conditions used here. This results in an almost total quenching of its PL and electrical transport properties. In contrast, fully inorganic cesium-based NCs exhibit a significantly enhanced stability than their hybrid counterpart. Indeed, although the PL is partly quenched by the removal of surface ligands, almost 50 % of the initial PLQY is maintained even after 15 minutes of oxygen plasma at 50 W. Furthermore, although electrical conductivity of $CsPbBr_3$ NC films is diminished upon exposure to oxygen plasma, the films show a more ohmic behavior with linear current-voltage curves and almost no hysteresis in contrast with pristine films.

ASSOCIATED CONTENT

Supporting Information. Experimental details, TEM, absorption and photoluminescence spectra of NCs in solution, XPS spectra, XRD of thin films, PL spectra of thin films.

AUTHOR INFORMATION

Corresponding Author

*E-mail: Francisco.palazon@uv.es

*E-mail: Liberato.manna@iit.it

Notes

The authors declare no competing financial interest.

ACKNOWLEDGMENT

F. P. acknowledges the European Union Framework Programme for Research and Innovation Horizon 2020 (2014-2020) under the Marie Skłodowska-Curie Grant Agreement PerovSAMs No. 747599. Q.A., M.I. and L. M. acknowledge the European Union seventh Framework Programme under Grant Agreement No. 614897 (ERC Consolidator Grant "TRANS-NANO").

REFERENCES

(1) Sun, J.; Yang, J.; Lee, J. I.; Cho, J. H.; Kang, M. S. Lead-Free Perovskite Nanocrystals for Light-Emitting Devices. *J. Phys. Chem. Lett.* **2018**, *9*, 1573–1583.

(2) Kim, Y. H.; Wolf, C.; Kim, Y. T.; Cho, H.; Kwon, W.; Do, S.; Sadhanala, A.; Park, C. G.; Rhee, S. W.; Im, S. H.; Friend, R.; Lee, T-W. Highly Efficient Light-Emitting Diodes of Colloidal Metal-Halide Perovskite Nanocrystals beyond Quantum Size. *ACS Nano* **2017**, *11*,

6586–6593.

(3) Chin, X. Y.; Perumal, A.; Bruno, A.; Yantara, N.; Veldhuis, S. A.; Martínez-Sarti, L.; Chandran, B.; Chirvony, V.; Lo, A. S. Z.; So, J.; Soci, C.; Grätzel, M.; Bolink, H.J.; Mathews, N; Mhaisalkar, S.G. Self-Assembled Hierarchical Nanostructured Perovskites Enable Highly Efficient LEDs: Via an Energy Cascade. *Energy Environ. Sci.* **2018**, *11*, 1770–1778.

(4) Chiba, T.; Hoshi, K.; Pu, Y. J.; Takeda, Y.; Hayashi, Y.; Ohisa, S.; Kawata, S.; Kido, J. High-Efficiency Perovskite Quantum-Dot Light-Emitting Devices by Effective Washing Process and Interfacial Energy Level Alignment. *ACS Appl. Mater. Interfaces* **2017**, *9*, 18054–18060.

(5) Wang, H. C.; Bao, Z.; Tsai, H. Y.; Tang, A. C.; Liu, R. S. Perovskite Quantum Dots and Their Application in Light-Emitting Diodes. *Small* **2018**, *14*, 1–23.

(6) Shan, Q.; Li, J.; Song, J.; Zou, Y.; Xu, L.; Xue, J.; Dong, Y.; Huo, C.; Chen, J.; Han, B.; Zeng, H. All-Inorganic Quantum-Dot Light-Emitting Diodes Based on Perovskite Emitters with Low Turn-on Voltage and High Humidity Stability. *J. Mater. Chem. C* **2017**, *5*, 4565–4570.

(7) Kim, Y. H.; Lee, G. H.; Kim, Y. T.; Wolf, C.; Yun, H. J.; Kwon, W.; Park, C. G.; Lee, T. W. High Efficiency Perovskite Light-Emitting Diodes of Ligand-Engineered Colloidal Formamidinium Lead Bromide Nanoparticles. *Nano Energy* **2017**, *38*, 51–58.

(8) Gangishetty, M. K.; Hou, S.; Quan, Q.; Congreve, D. N. Reducing Architecture Limitations for Efficient Blue Perovskite Light-Emitting Diodes. *Adv. Mater.* **2018**, *1706226*, 1–6.

(9) Lignos, I.; Morad, V.; Shynkarenko, Y.; Bernasconi, C.; Maceiczyk, R. M.; Protesescu, L.; Bertolotti, F.; Kumar, S.; Ochsenbein, S. T.; Masciocchi, N.; Guagliardi, A.; Shih, C-J.; Bodnarchuk, M. I.; deMello, A. J.; Kovalenko, M. Exploration of Near-Infrared-Emissive Colloidal Multinary Lead Halide Perovskite Nanocrystals Using an Automated Microfluidic Platform. *ACS Nano* **2018**, *12*, 5504–5517.

(10) Akkerman, Q. A.; Gandini, M.; Di Stasio, F.; Rastogi, P.; Palazon, F.; Bertoni, G.; Ball, J. M.; Prato, M.; Petrozza, A.; Manna, L. Strongly Emissive Perovskite Nanocrystal Inks for High-Voltage Solar Cells. *Nat. Energy* **2017**, *2*, 141–153.

(11) Bian, H.; Bai, D.; Jin, Z.; Wang, K.; Liang, L.; Wang, H.; Zhang, J.; Wang, Q.; Liu, S. (Frank). Graded Bandgap CsPbI2+xBr1−xPerovskite Solar Cells with a Stabilized Efficiency of 14.4%. *Joule* **2018**, 1–11.

(12) Swarnkar, A.; Marshall, A. R.; Sanehira, E. M.; Chernomordik, B. D.; Moore, D. T.; Christians, J. A.; Chakrabarti, T.; Luther, J. M. Quantum Dot–induced Phase Stabilization of A-CsPbI3 Perovskite for High-Efficiency Photovoltaics Abhishek. *Science (80-.).* **2016**, *354*, 92–95.

(13) Sanehira, E. M.; Marshall, A. R.; Christians, J. A.; Harvey, S. P.; Ciesielski, P. N.; Wheeler, L. M.; Schulz, P.; Lin, L. Y.; Beard, M. C.; Luther, J. M. Enhanced Mobility $CsPbI_3$ Quantum Dot Arrays for Record-Efficiency, High-Voltage Photovoltaic Cells. *Sci. Adv.* **2017**, *3*, 4204.

(14) Christodoulou, S.; Di Stasio, F.; Pradhan, S.; Stavrinadis, A.; Konstantatos, G. High Open Circuit Voltage Solar Cells Based on Bright Mixed-Halide $CsPbBrI_2$ Perovskite Nanocrystals Synthesized in Ambient Air Conditions. *J. Phys. Chem. C* **2018**, *122*, 7621–7626.

(15) Ahmadian-Yazdi, M. R.; Eslamian, M. Fabrication of Semiconducting Methylammonium Lead Halide Perovskite Particles by Spray Technology. *Nanoscale Res. Lett.* **2018**, *13*, 4–11.

(16) Elgamel, H. E. A. High Efficiency Polycrystalline Silicon Solar Cells Using Low Temperature PECVD Process. *IEEE Trans. Electron Devices* **1998**, *45*, 2131–2137.

(17) Iwahashi, T.; Morishima, M.; Fujibayashi, T.; Yang, R.; Lin, J.; Matsunaga, D. Silicon Nitride Anti-Reflection Coating on the Glass and Transparent Conductive Oxide Interface for Thin Film Solar Cells and Modules. *J. Appl. Phys.* **2015**, *118*.

(18) Jin, M. J.; Jo, J.; Neupane, G. P.; Kim, J.; An, K. S.; Yoo, J. W. Tuning of Undoped ZnO Thin Film via Plasma Enhanced Atomic Layer Deposition and Its Application for an Inverted Polymer Solar Cell. *AIP Adv.* **2013**, *3*.

(19) Hodgkinson, J. L.; Yates, H. M.; Walter, A.; Sacchetto, D.; Moon, S. J.; Nicolay, S. Roll to Roll Atmospheric Pressure Plasma Enhanced CVD of Titania as a Step towards the Realisation of Large Area Perovskite Solar Cell Technology. *J. Mater. Chem. C* **2018**, *6*, 1988–1995.

(20) Zardetto, V.; Di Giacomo, F.; Lucarelli, G.; Kessels, W. M. M.; Brown, T. M.; Creatore, M. Plasma-Assisted Atomic Layer Deposition of TiO_2 compact Layers for Flexible Mesostructured Perovskite Solar Cells. *Sol. Energy* **2017**, *150*, 447–453.

(21) Ma, X.; Tang, P.; Liu, D.; Zhang, J.; Feng, L.; Wu, L. Interface Engineering of Perovskite Solar Cells with Air Plasma Treatment for Improved Performance. *ChemPhysChem* **2017**, *18*, 2939–2946.

(22) Wang, C.; Zhao, D.; Grice, C. R.; Liao, W.; Yu, Y.; Cimaroli, A.; Shrestha, N.; Roland, P. J.; Chen, J.; Yu, Z.; Liu, P.; Cheng, N.; Ellingson, R. J.; Zhao, X.; Yan, Y. Low-Temperature Plasma-Enhanced Atomic Layer Deposition of Tin Oxide Electron Selective Layers for Highly Efficient Planar Perovskite Solar Cells. *J. Mater. Chem. A* **2016**, *4*, 12080–12087.

(23) Xiao, X.; Bao, C.; Fang, Y.; Dai, J.; Ecker, B. R.; Wang, C.; Lin, Y.; Tang, S.; Liu, Y.; Deng, Y.; Zheng, X.; Gao, Y.; Zeng, X. Ch.; Huang, J. Argon Plasma Treatment to Tune Perovskite Surface Composition for High Efficiency Solar Cells and Fast Photodetectors. *Adv. Mater.* **2018**, *30*, 1–7.

(24) Loiudice, A.; Saris, S.; Oveisi, E.; Alexander, D. T. L.; Buonsanti, R. CsPbBr 3 QD/AlO x Inorganic Nanocomposites with Exceptional Stability in Water, Light, and Heat. *Angew. Chemie Int. Ed.* **2017**, *56*, 10957–10957.

(25) Palazon, F.; Akkerman, Q. A.; Prato, M.; Manna, L. X-Ray Lithography on Perovskite Nanocrystals Films: From Patterning with Anion-Exchange Reactions to Enhanced Stability in Air and Water. *ACS Nano* **2016**, *10*, 1224–1230.

(26) Palazon, F.; Almeida, G.; Akkerman, Q. A.; De Trizio, L.; Dang, Z.; Prato, M.; Manna, L. Changing the Dimensionality of Cesium Lead Bromide Nanocrystals by Reversible Postsynthesis Transformations with Amines. *Chem. Mater.* **2017**, *29*, 4167–4171.

(27) Udayabhaskararao, T.; Houben, L.; Cohen, H.; Menahem, M.; Pinkas, I.; Avram, L.; Wolf, T.; Teitelboim, A.; Leskes, M.; Yaffe, O.; Oron, D.; Kazes, M. A Mechanistic Study of Phase Transformation in Perovskite Nanocrystals Driven by Ligand Passivation. *Chem. Mater.* **2018**, *30*, 84–93.

(28) Liu, Z.; Bekenstein, Y.; Ye, X.; Nguyen, S. C.; Swabeck, J.; Zhang, D.; Lee, S. T.; Yang, P.; Ma, W.; Alivisatos, A. P. Ligand Mediated Transformation of Cesium Lead Bromide Perovskite Nanocrystals to Lead Depleted Cs4PbBr6Nanocrystals. *J. Am. Chem. Soc.* **2017**, *139*, 5309–5312.

(29) Diroll, B. T.; Nedelcu, G.; Kovalenko, M. V.; Schaller, R. D. High-Temperature Photoluminescence of $CsPbX_3$ (X = Cl, Br, I) Nanocrystals. *Adv. Funct. Mater.* **2017**, *27*, 1606750.

(30) Palazon, F.; Dogan, S.; Marras, S.; Locardi, F.; Nelli, I.; Rastogi, P.; Ferretti, M.; Prato, M.; Krahne, R.; Manna, L. From $CsPbBr_3$ Nano-Inks to Sintered $CsPbBr_3$ –$CsPb_2Br_5$ Films via Thermal Annealing: Implications on Optoelectronic Properties. *J. Phys. Chem. C* **2017**, *121*, 11956–11961.

(31) Palazon, F.; Di Stasio, F.; Lauciello, S.; Krahne, R.; Prato, M.; Manna, L. Evolution of $CsPbBr_3$ Nanocrystals upon Post-Synthesis Annealing under an Inert Atmosphere. *J. Mater. Chem. C* **2016**, *4*, 9179–9182.

(32) Imran, M.; Caligiuri, V.; Wang, M.; Goldoni, L.; Prato, M.; Krahne, R.; De Trizio, L.; Manna, L. Benzoyl Halides as Alternative Precursors for the Colloidal Synthesis of Lead-Based Halide Perovskite Nanocrystals. *J. Am. Chem. Soc.* **2018**, *140*, 2656–2664.

(33) Zorn, G.; Dave, S. R.; Gao, X.; Castner, D. G. Method for Determining the Elemental Composition and Distribution in Semiconductor Core-Shell Quantum Dots. *Anal. Chem.* **2011**, *83*, 866–873.

(34) Juarez-Perez, E. J.; Ono, L. K.; Maeda, M.; Jiang, Y.; Hawash, Z.; Qi, Y. Photodecomposition and Thermal Decomposition in Methylammonium Halide Lead Perovskites and Inferred Design Principles to Increase Photovoltaic Device Stability. *J. Mater. Chem. A* **2018**, *6*, 9604–9612.

Insert Table of Contents artwork here